Journal of Materials Science: Materials in Electronics (2019) 30:7704–7710
https://doi.org/10.1007/s10854-019-01086-6

Study on leakage current, ferroelectric and dielectric properties of BFMO thin films with different bismuth contents

L. X. Chen[1] · C. Xu[1] · X. L. Fan[1] · X. H. Cao[1] · K. Ji[1] · C. H. Yang[1]

Received: 24 December 2018 / Accepted: 6 March 2019 / Published online: 12 March 2019

Abstract

$Bi_{(1+x)}Fe_{0.95}Mn_{0.05}O_3$ thin films with different bismuth contents (abbreviated as $B_{1+x}FMO$, $x = -0.05, 0, 0.05, 0.1$) were fabricated by chemical solution deposition on ITO/glass substrates. The effects of Bi nonstoichiometry on the microstructure, leakage current, ferroelectric and dielectric properties of BFMO films are investigated. The $B_{1.05}FMO$ and $B_{1.1}FMO$ thin films possess single perovskite structure, while the secondary phase of $Bi_2Fe_4O_9$ can be observed in BFMO and $B_{0.95}FMO$ thin films. Compared with the other three samples in this work, drastically reduced leakage current can be found in $B_{1.05}FMO$. For each film, the dominant conduction mechanisms are the Ohmic conduction and the space charge limited conduction at lower electric fields and the interface-limited Fowler–Nordheim tunneling at higher electric regions, respectively. Among the $B_{1+x}FMO$ films ($x = -0.05, 0, 0.05, 0.1$), the $B_{1.05}FMO$ film possesses significantly improved electrical properties, reflected by a large remanent polarization ($P_r \sim 68.3$ μC/cm^2), lower dielectric loss ($\tan\delta \sim 0.02$), large dielectric constant ($\varepsilon_r \sim 210$) and high tunability (88%). These results suggest that the 5 mol% excess of Bi is the prior content to get better insulation, optimize ferroelectric as well as dielectric properties of $BiFeO_3$ film, giving reference to modify electrical performances of ferroelectric materials through regulation of volatile element.

1 Introduction

Lead-based ferroelectric materials, on behalf of $Pb(Zr,Ti)O_3$ and $Pb(Mg,Nb)O_3$, have been extensively studied due to the excellent ferroelectric properties [1, 2]. Nevertheless, there is a serious problem that the toxic Pb hampers human health and environment protection, which have attracted considerable attention. In this case, studies concerning about lead-free ferroelectric materials, represented by $BiFeO_3$ (BFO), $(K_{0.5}Na_{0.5})NbO_3$ (KNN), and $Na_{0.5}Bi_{0.5}TiO_3$ (NBT)-based film systems [3–5], have been moved to the forefront of ferroelectric material research, and great progresses in synthesis and characterization in the studies of these materials have been made so far. Taking the lead-free NBT film for example, researches dealing with the leakage problem of pure NBT thin films have been conducted to improve the electrical properties since its report in 2004 [6], methods of which include cation substitution, controlling of orientation and making solid solutions with other components such as $BaTiO_3$ [7–9], commonly used methods in modifying the structural and electrical properties of ferroelectrics.

BFO, with large theoretical remanent polarization P_r ~ 100 μC/cm^2 and ultra-high Curie temperature ($T_c = 1103$ K) [10], has potential in the field of electrical devices including ferroelectric resistive memory [11], energy harvester [12], rechargeable batteries [13]. Also, it can be applied as flexible multistate high-storage memory device with an ITO/$BiFeO_3$/Ti/Polyimide structure for light-controlled simultaneous resistive and ferroelectricity switching effects [14].

Ferroelectric materials in form of film have the advantages of low crystallization temperature, small size and ease of integration in comparison to ceramics. However, the high leakage current severely limit the practical application of BFO thin films, which is attributed to large quantities of free oxygen vacancies $(V_{O^{2-}})^{\cdot\cdot}$ formed by the volatilization of Bi element and valence fluctuation of Fe^{3+} during heat treatment. The site-engineering is an effective strategy to enhance the electrical performances in BFO-based materials [15]. Considering that the radius of Mn^{2+} (0.80 Å) is much lower than that of Bi^{3+} (1.02 Å), but very close to that of Fe^{3+} (0.64 Å), combined with the principles of crystal chemistry, Mn^{2+} should be induced as B-site doping ions in BFO. In this

✉ C. H. Yang
mse_yangch@ujn.edu.cn

[1] School of Materials Science and Engineering, University of Jinan, Jinan 250022, China

work, as acceptor dopant, 5 mol% Mn was doped in BFO thin film to get better insulation [16]. Some other researches have also been carried out to overcome deterioration in electrical properties induced by the leakage problem in BFO film. For example, Ren et al. reported that the leakage current density in 5 mol% Bi excess modified BFO thin film annealed at 715 °C was drastically decreased to 10^{-6} A/cm^2 at 200 kV/cm [17]. Hu et al. have mentioned that $Bi_{0.97}Gd_{0.03}FeO_3$ thin film annealed at 550 °C, with 2 at.% excess bismuth added, exhibited a well-defined polarization–electric (*P–E*) with P_r ~ 79 μC/cm^2 [18]. Chai et al. have also found that 5 mol% Bi excessive $Bi_{0.88}Sr_{0.03}Gd_{0.09}Fe_{0.94}Mn_{0.04}Co_{0.02}O_3$ thin film after annealing at 550 °C displayed excellent ferroelectric properties manifested as a giant remanent polarization of P_r ~ 108 μC/cm^2 [19].

In the light of this, it is significant to add excess Bi in precursor solution to compensate for Bi loss in the high-temperature crystallization of BFO thin films. It is widely known that the crystallization and electrical performances of ferroelectric films should be strongly dependent on the annealing temperature. Under a certain preparation environment, each ferroelectric thin film material has its own optimal crystallization temperature. For example, Zhang et al. have reported that $0.94Na_{0.5}Bi_{0.5}TiO_3$–$0.06BaTiO_3$ thin film annealed at 450 °C has higher electric break-down field strength (3310 kV/cm) than other temperatures [20]. Yan et al. have mentioned that La-doped BFO thin film annealed at 525 °C exhibits higher remanent polarization (P_r = 72.9 μC/cm^2) [21]. Likewise, BFO should have a most suitable Bi content under a certain annealing temperature. However, seeing that different contents of Bi excess (2 mol%, 5 mol%) were commonly added in BFO-based films even at the same annealing temperature (550 °C) [18, 19], it is necessary to conduct systematic study of Bi nonstoichiometry to explore the optimal composition content for BFO. Taking the reported works and our previous experience as references, an appropriate annealing temperature of 540 °C was chosen as the annealing temperature for the 5 mol% Mn-doped BFO in this work. The chemical solution decomposition (CSD) method takes the advantages of chemical homogeneity, easy stoichiometry control and integration into devices as well as low cost, which has been widely used in the preparing process for ferroelectric thin films [4, 5].

Based on the mentioned above, Mn-substituted BFO thin films ($Bi_{1+x}Fe_{0.95}Mn_{0.05}O_3$, B_{1+x}FMO) with different bismuth contents [(− 5) to (+ 10) mol%] were prepared by chemical solution deposition (CSD) on ITO/glass substrates. The influences of Bi excess on the structure, leakage current, ferroelectric and dielectric properties of Mn-doped BFO films were investigated. Among all the B_{1+x}FMO film samples, the lowest leakage current density and a saturated *P–E* loop (P_r ~ 68.3 μC/cm^2) can be observed in the $B_{1.05}$FMO thin film, which originates from its pure phase structure and dense microstructure.

2 Experimental

5 mol% Mn doped $Bi_{1+x}FeO_3$ (B_{1+x}FMO, x = − 0.05, 0, 0.05, 0.1) thin films were deposited on ITO/glass substrates by CSD. To prepare the precursor solution, $Bi(NO_3)_3{\cdot}5H_2O$, $Fe(NO_3)_3{\cdot}9H_2O$ and $C_4H_6O_4Mn{\cdot}4H_2O$ were selected as raw materials dissolving in ethylene glycol and acetic acid, and a moderate amount of acetylacetone was added as stabilizing reagent. At last, polyethylene glycol (PEG) was mixed in the solution mentioned above to fine-tune the uniformity of the final solution. After constant stirring, the transparent and stable precursor solution with the concentration of 0.3 M was acquired. Keeping the other process parameters constant and adding different amounts of bismuth nitrate into the solutions, four precursor solutions with slight variations in bismuth [(− 5) to (+ 10) mol% of Bi] were prepared. Each precursor solution was spin-coated on ITO/glass substrates at 3000 rpm for 30 s. The fabricated wet films were pyrolyzed at 300 °C on a hot plate for 3 min and the dried films were annealed at 540 °C for 20 min on a hot plate in the air atmosphere for the complete crystallization. These deposition and heat treatment procedures were repeated several times to acquire the desired thickness of B_{1+x}FMO thin films.

The crystallinity of B_{1+x}FMO thin films was characterized using X-ray diffraction (XRD, Bruker D8). The microscopic morphologies and cross-sectional images of the films were detected by field emission scanning electron microscopy (FeSEM, Hitachi S-4200). The X-ray photoelectron spectroscopy (XPS) were recorded a PHI 5000 VersaProbe XPS instrument (Thermo ESCALAB 250XI). The ferroelectric properties were measured by a qualified ferroelectric tester (Precision Pro. Radiant Technologies). The leakage current was conducted through a semiconductor characterization system (Keithley 4200). The dielectric properties were tested using an impedance analyzer (HP4294A).

3 Results and discussion

Figure 1 shows the XRD patterns of B_{1+x}FMO (x = − 0.05, 0, 0.05, 0.1) thin films deposited on ITO/glass substrates. The $B_{1.05}$FMO & $B_{1.1}$FMO thin films possess single perovskite structure with rhombohedral symmetry. Nevertheless, the secondary phase of $Bi_2Fe_4O_9$ at about 2θ = 28° and 33° is distinctly observed in the BFMO and $Bi_{0.95}$FMO thin film. This phenomenon can be usually found in the Bi-deficient BFO-based thin film [22]. From the result of XRD, it can be speculated that excess Bi is conducive to

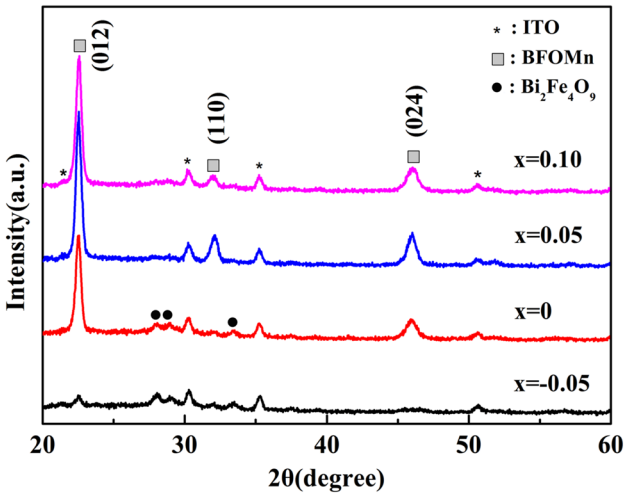

Fig. 1 XRD patterns of $B_{1+x}FMO$ (x = −0.05, 0, 0.05, 0.1) thin films

suppressing the generation of impurity phase and improving the crystallization.

Generally, for BFO thin films, the leakage problem mainly caused by oxygen vacancies [23]. As described by the following equations, oxygen vacancies are mainly introduced by the reductions of Fe^{3+} to Fe^{2+} and the deficiencies of Bi ions in NBT–BT–BFO films, which can lead to a large leakage current:

$$2Fe_{Fe} + O_O \rightarrow 2Fe'_{Fe} + V_O^{\cdot\cdot} + \frac{1}{2}O_2 \quad (1)$$

$$2Bi_{Bi} + 3O_O \rightarrow 2V_{Bi}^{'''} + 3V_O^{\cdot\cdot} + Bi_2O_3 \quad (2)$$

To evaluate the valence states of the Fe and Mn ions in the $B_{1.05}FMO$ film, the XPS for Fe 2p and Mn 2p core level binding energy spectra of is presented. From Fig. 2a and b, the coexistences of Fe^{3+} and Fe^{2+} as well as Mn^{3+} and Mn^{2+} can be found, where the fractions of Fe^{3+}/Fe^{2+} and Mn^{3+}/Mn^{2+} are 74%/26% and 61%/39%, respectively. This suggests the changes in the valence state of Fe^{3+} and Mn^{2+}. In the $B_{1.05}FMO$ film, with the oxidations of Mn^{2+}, some of oxygen vacancies were filled up to maintain the charge balance, and the reaction proceed by:

$$2Mn'_{Fe} + V_O^{\cdot\cdot} + \frac{1}{2}O_2 \rightarrow 2Mn_{Fe} + O_O \quad (3)$$

Therefore, the content of oxygen vacancies is reduced and the resistivity is improved by Mn doping. Similar results have been achieved in other BFO-based material [24].

The leakage current densities of BFMO films were characterised by the *J*–*E* curves in Fig. 3a. It can be seen from Fig. 3a that all these BFMO thin films show asymmetry between the positive and negative applied electric fields. It may be related to the different interface state between the bottom ITO/BFO and the top Au/BFO [25]. The leakage current density of a series of $B_{1+x}FMO$ thin films has a nonlinear raising trend with the increase of applied electric field. Moreover, descending leakage current density is presented with the increasing excess Bi content for $x \leq 0.05$ under the same applied electric field. The main reason is that the volatilization of bismuth ions can be compensated by the overdosed Bi content. However, the leakage current density will increase when the excess Bi content over 5 mol%. The reason for this phenomenon maybe that excess Bi forms impurity phase which provides a tunnel for leakage current [26]. A similar phenomenon in pure BFO thin film was also reported by Yan et al. [27]. In this work, $B_{1.05}FMO$ has the most improved resistivity, which should be attributed to its few oxygen vacancies and relatively good crystallization

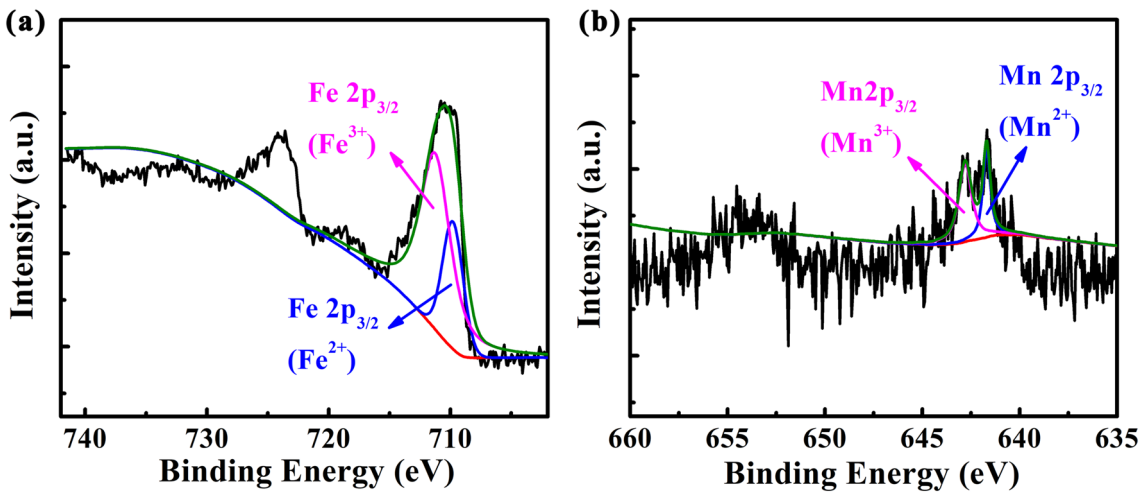

Fig. 2 XPS for **a** Fe and **b** Mn elements of $B_{1.05}FMO$ film

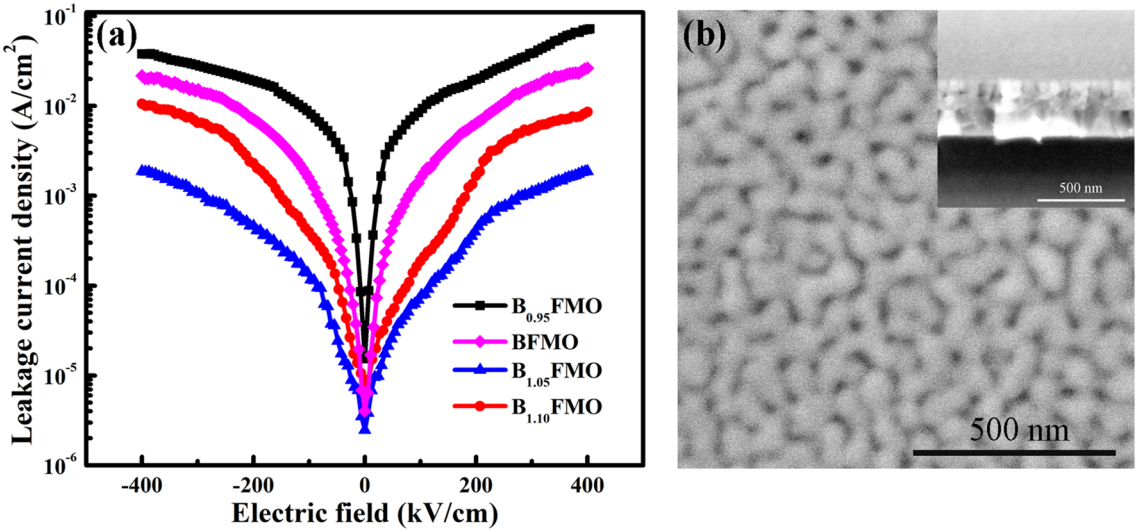

Fig. 3 **a** Leakage current density (J) as a function of the electric field (E) for $B_{1+x}FMO$ (x = − 0.05, 0, 0.05, 0.1) film, **b** SEM images of the surface morphology and cross-section diagram of $B_{1.05}FMO$ film

(as shown in Fig. 3b). The low leakage current density of $B_{1.05}FMO$ (1.61×10^{-4} A/cm^2 at 200 kV/cm) is one order of magnitude smaller than other BFO based thin film at the same E [28].

By fitting J–E data, the conduction mechanisms of $B_{1+x}FMO$ (x = − 0.05, 0, 0.05, 0.1) thin films in leakage current have been studied. In view of that the space charge limited conduction (SCLC) usually occurs in the ferroelectric materials, Fig. 4a gives the plots of log(J)–log(E) based on the following equation [29]:

$$JSCLC = \frac{9\mu\varepsilon_r\varepsilon_0}{8d}E^2$$

where J is leakage current density, ε_r is the relative dielectric constant, μ is the charge carrier mobility, d is the film thickness, ε_0 is the permittivity of free space and E is the applied electric field. At low applied E region, the values of relative slope α are 1.11, 1.18, 0.91 and 1.06, respectively suggesting that the leading effect of Ohmic conduction in the initial stage. For each film, the value of α is around 2 when the log(E) is in the range of 6.5–7.0 V/m. This indicates that leakage behavior of $B_{1+x}FMO$ (x = − 0.05, 0, 0.05, 0.1) is taken charge of by the SCLC mechanism. The Similar phenomenon was also observed in Ba and Nb substituted BFO film [30]. This stems from the fact that the applied E causes electrons to be injected into thin films, resulting in more carriers injected from the electrodes than the bulk-generated carriers. With the continuous increase of E, these films possess greater values of α much over 2. Therefore, considering the interface-limited Fowler–Nordheim (FN) tunneling is taken into consideration as given by the following equation [29]:

$$J_{FN} = CE^2 e^{-\frac{D^2\sqrt{\phi_i^3}}{E}}$$

where J is leakage current density, φ_i is the potential barrier height, C and D are constants and E is the applied electric field. As shown in Fig. 4b, a linear relation between Ln(J/E^2) and 1/E of these thin films at high E regions can be observed, which reveals that the leakage behaviour is dominated by FN tunneling mechanism under high applied E region. Therefore, the insulating characteristics of each $B_{1+x}FMO$ thin film is dominant by the Ohmic conduction and SCLC at low E, and FN tunneling at high E regions.

Figure 5 exhibits the polarization–electric field (P–E) hysteresis loops of $B_{1+x}FMO$ (x = − 0.05, 0, 0.05, 0.1) thin films, which were measured under the frequency of 10 kHz and at room temperature. One can find that the BFMO samples with − 5 mol% and 0 mol% excess content of Bi show the obvious feature with the round shape at the positive applied electric fields. This may be owing to the high leakage current resulting from the formation of the secondary phase and the oxygen vacancy. The samples of $B_{1.05}FMO$ and $B_{1.1}FMO$ exhibit well-defined P–E loops. For clarity, the values of remanent polarization (P_r) and coercive field (E_c) at 778 kV/cm for the films as functions of excess Bi are shown in Fig. 6. When the content of excess Bi is 5 mol%, the value of P_r reaches 55.5 μC/cm^2, which is larger than that of $Bi_{0.9}Eu_{0.1}FeO_3$ thin film (P_r = 44.75 μC/cm^2) and comparable to that of BFO206/BGFO150 layer thin film (P_r = 68.85 μC/cm^2) [31, 32]. Furthermore, one can discover that the E_c of $B_{1.05}FMO$ thin film is the minimum (531 kV/cm) among all the samples, which can be attributed to the decrease of defects.

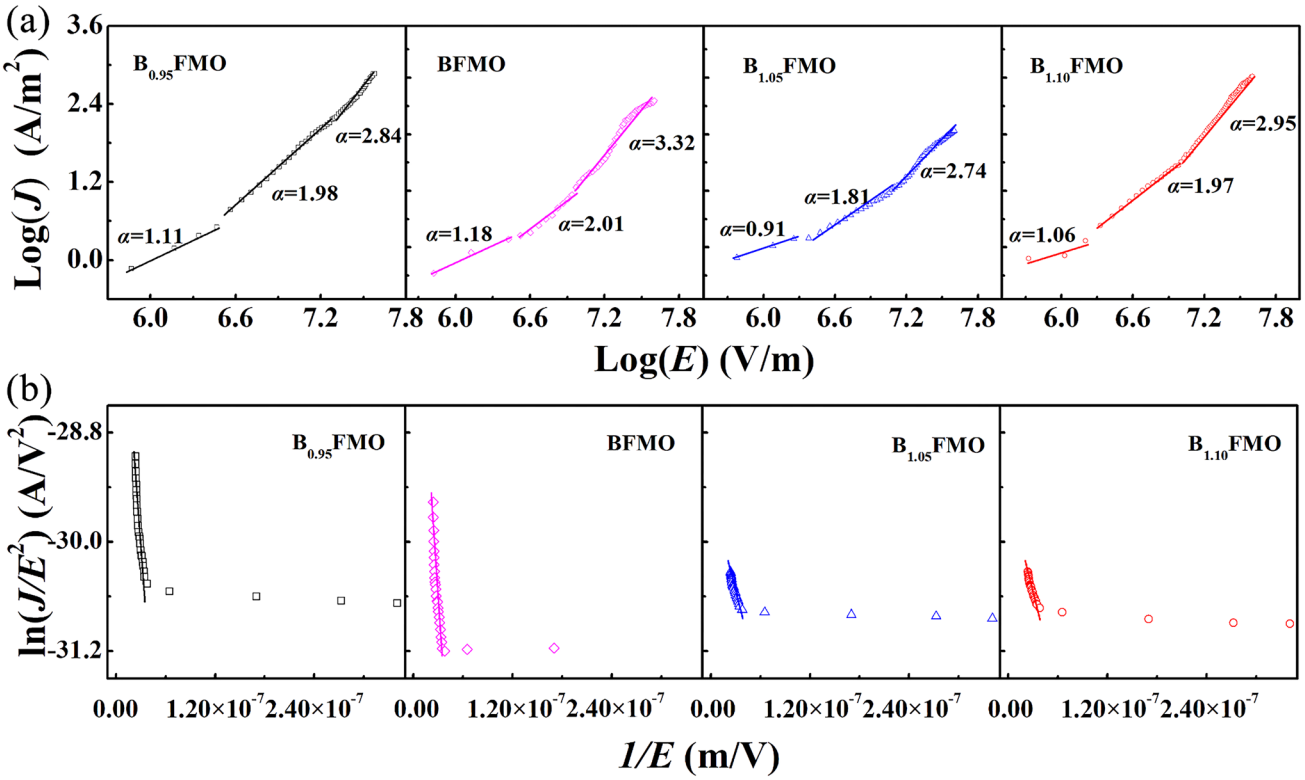

Fig. 4 Plots of leakage current conduction mechanism for $B_{1+x}FMO$ (x = −0.05, 0, 0.05, 0.1) thin films: **a** Log(*J*)–Ln(*E*), **b** Ln(J/E^2)–1/*E*

Therefore, the ferroelectric performance of BFMO-based film is sensitive to the Bi content.

Figure 7 exhibits the room temperature frequency dependent dielectric constant (ε_r) and dielectric loss (tanδ) of $B_{1+x}FMO$ (x = −0.05, 0, 0.05, 0.1) thin films in the range of 1 kHz to 1 MHz. For each film, the value of ε_r decreases slowly with the frequency increasing. This stems from the fact that the polarization cannot occur instantaneously at high frequency. As Bi content increases, one can observe that the ε_r increases first and then decreases. And then, the tanδ descends slowly and then raises with the growth of frequency, which may be owing to the tanδ is prior affected by leakage current at low frequency region and dipole inertia is a major contributor to the dissipation factor at high frequency region. When the excess content of Bi is 5 mol%, the values of ε_r and tanδ reach 210 and 0.02 at an applied frequency of 100 kHz, respectively. One can find that the ε_r and the tanδ are superior to $Bi_{0.9}Dy_{0.1}Fe_{0.975}Zn_{0.025}O_3$ thin film (ε_r = 81, tanδ = 0.035) [33, 34].

According to the above research, the 5 mol% Bi-doped film has a larger remnant polarization and a smaller leakage current than other Bi doping samples. Figure 8 shows the normalized *C*–*V* curve of the $B_{1.05}FMO$ thin film. The curve features butterfly-type shape because of the switching of ferroelectric domains, which proves the thin film has better ferroelectricity. The *C*–*V* curve doesn't show symmetry about *V* = 0. It may be resulted from the difference of the work function between the bottom electrode and the top electrode. The tunability (*T*) reflects the ability to operate dielectric permittivity by electric fields and the tunability is defined by:

$$T(\%) = \frac{(C_{\max} - C_E)}{C_{\max}} \times 100\%$$

where the C_E is the capacitance under the applied electric fields and the C_{max} is the maximum capacitance. As a result, a maximum tunability of 88% was calculated. The higher tunability allows $B_{1.05}FMO$ thin films to be better used in microwave applications like matching networks and tunable filters, etc [35].

4 Conclusion

To sum up, the 5 mol% Mn doped $Bi_{1+x}FeO_3$ ($B_{1+x}FMO$, x = −0.05, 0, 0.05, 0.1) thin films were grown on ITO/glass substrates by chemical solution deposition. The consequences manifest that the Bi nonstoichiometry plays a crucial part in the electric performance of $B_{1+x}FMO$ films. Among a series of samples, the $B_{1.05}FMO$ film has the lowest leakage current of 1.61×10^{-4} A/cm^2 at 200 kV/cm,

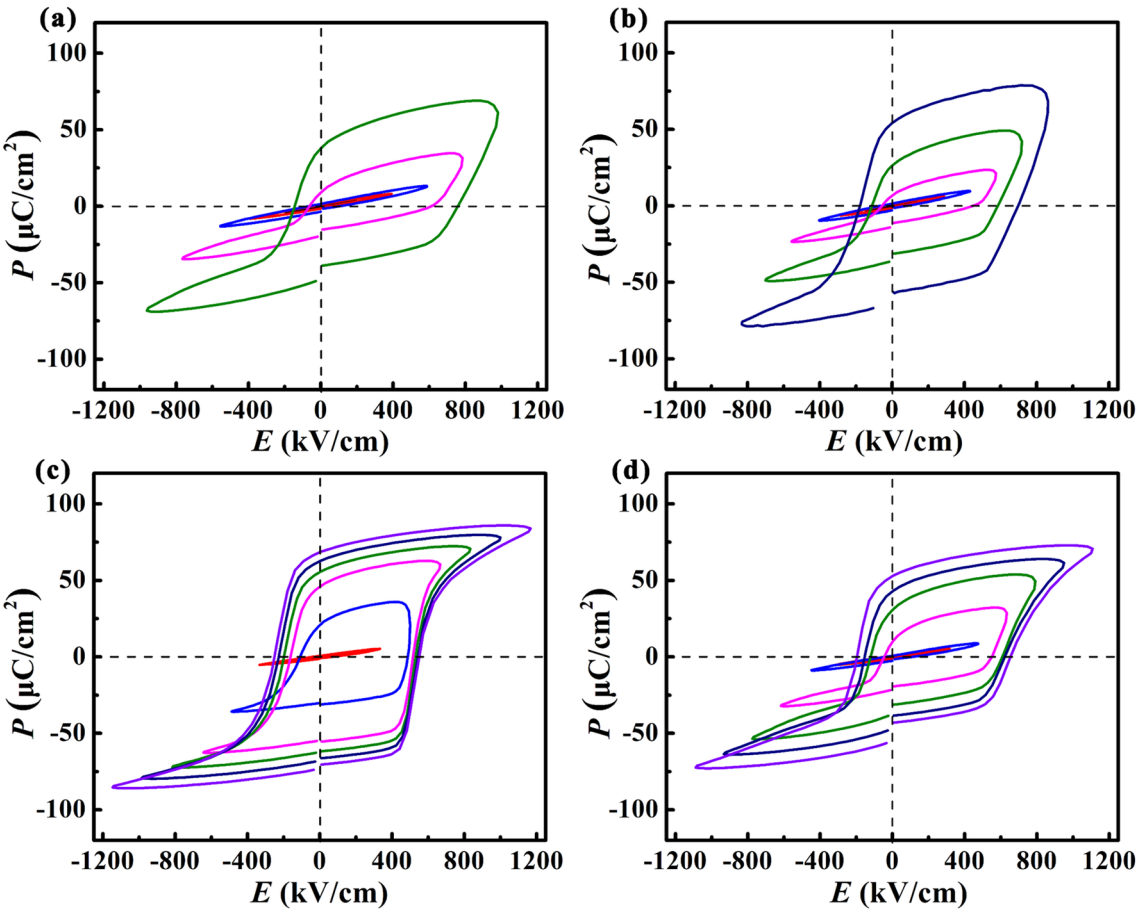

Fig. 5 The *P*–*E* hysteresis loops of $B_{1+x}FMO$ (x = − 0.05, 0, 0.05, 0.1) thin films

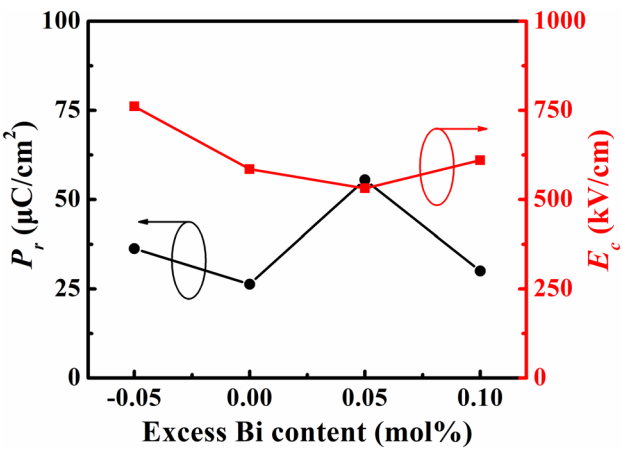

Fig. 6 P_r and E_c values as functions of excess Bi content annealed

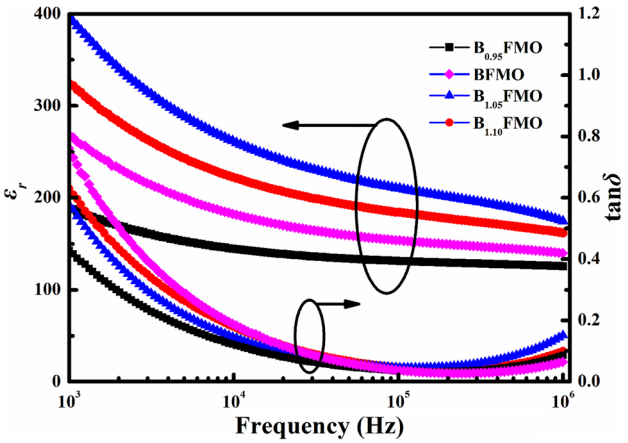

Fig. 7 ε_r and tanδ as functions of frequency for $B_{1+x}FMO$ (x = − 0.05, 0, 0.05, 0.1) thin films

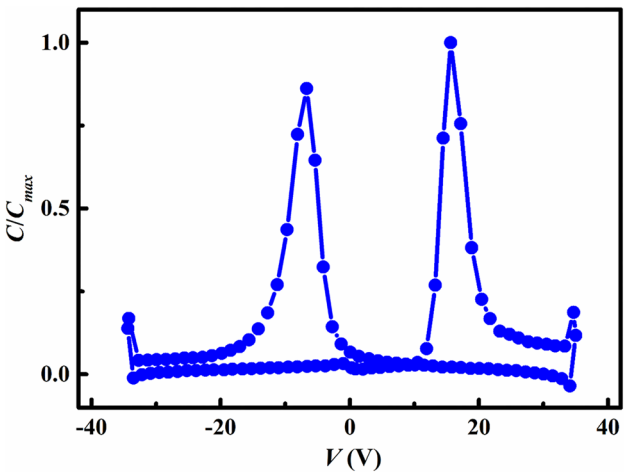

Fig. 8 C/C_{max}–V curve of $B_{1.05}$FMO thin film

a larger remanent polarization (P_r ~ 68.3 μC/cm^2), larger dielectric constant (~ 210), lower dielectric loss (~ 0.02) and larger tunability (88%). On basis of the experiment consequences, moderate Bi excess is testified to be feasible and workable to improve the electrical properties for BFO-based thin films.

Acknowledgements This work was supported by the Shandong Provincial Natural Science Foundation of China (ZR2017LEM008).

References

1. C.L. Jia, K.W. Urban, M. Alexe, D. Hesse, I. Vrejoiu, Science **331**, 1420–1423 (2011)
2. Z.J. Jiang, Y. Nahas, S. Prokhorenko, S. Prosandeev, D. Wang, J. Íñiguez, L. Bellaiche, Phys. Rev. B **97**, 104110 (2018)
3. J. Wang, J.B. Neaton, H. Zheng, V. Nagarajan, S.B. Ogale, B. Liu, D. Viehland, V. Vaithyanathan, D.G. Schlom, U.V. Waghmare, N.A. Spaldin, K.M. Rabe, M. Wuttig, R. Ramesh, Science **299**, 1719–1722 (2003)
4. C. Kang, J.-H. Park, D. Shen, H. Ahn, M. Park, D.-J. Kim, J. Sol-Gel Sci. Technol. **58**, 85–90 (2011)
5. M. Cerneaa, L. Trupinaa, C. Dragoi, B.S. Vasile, R. Truscac, J. Alloy Compd. **515**, 166–170 (2012)
6. Z.H. Zhou, J.M. Xue, W.Z. Li, J. Wang, Appl. Phys. Lett. **85**, 804 (2004)
7. M.M. Hejazi, E. Taghaddos, A. Safari, J. Mater. Sci. **48**, 3511–3516 (2013)
8. M. Bousquet, J.-R. Duclère, B. Gautier, A. Boulle, A. Wu, S. Députier, D. Fasquelle, F. Rémondière, D. Albertini, C. Champeaux, P. Marchet, M. Guilloux-Viry, P. Vilarinho, J. Appl. Phys. **111**, 104106 (2012)
9. B.L. Peng, Q. Zhang, X. Li, T.Y. Sun, H.Q. Fan, S.M. Ke, M. Ye, Y. Wang, W. Lu, H.B. Niu, J.F. Scott, X.R. Zeng, H.T. Huang, Adv. Electron Mater. **1**, 1500052 (2015)
10. J. Wang, J.B. Neaton, H. Zheng, V. Nagarajan, S.B. Ogale, B. Liu, D. Viehland, V. Vaithyanathan, 5 D.G. Schlom, U.V. Waghmare, N.A. Spaldin, K.M. Rabe, M. Wuttig, R. Ramesh, Science **299**, 1719–1722 (2003)
11. A.Q. Jiang, C. Wang, K.J. Jin, X.B. Liu, J.F. Scott, C.S. Hwang, T.A. Tang, H.B. Lu, G.Z. Yang, Adv. Mater. **23**, 1277–1281 (2011)
12. S. Murakami, T. Yoshimura, K. Satoh, K. Wakazono, K. Kariya, N. Fujimura, J. Phys. **476**, 012007 (2013)
13. B. Sun, S.S. Mao, S.H. Zhu, G.D. Zhou, Y.D. Xia, Y. Zhao, ACS Appl. Nano Mater. **1**, 1291–1299 (2018)
14. B. Sun, M. Tang, J. Gao, C.M. Li, Chemeletrochem **3**, 896–901 (2016)
15. H. Pan, Y. Zeng, Y. Shen, Y.-H. Lin, J. Ma, L.L. Lia, C.-W. Nan, J. Mater. Chem. A **5**, 5920–5926 (2017)
16. T. Kawae, Y. Terauchi, H. Tsuda, M. Kumeda, A. Morimoto, Appl. Phys. Lett. **94**, 112904 (2009)
17. Y. Ren, X.H. Zhu, C.Y. Zhang, J.L. Zhu, J.G. Zhu, D.Q. Xiao, Ceram. Int. **40**, 2489–2493 (2014)
18. G.D. Hu, X. Cheng, W.B. Wu, C.H. Yang, Appl. Phys. Lett. **91**, 232909 (2007)
19. Z.J. Chai, G.Q. Tan, Z.W. Yue, W. Yang, M.Y. Guo, H.J. Ren, A. Xia, M.T. Xue, Y. Liu, L. Lv, Y. Liu, J. Alloy Compd. **746**, 677–687 (2018)
20. Y.L. Zhang, W.L. Li, W.P. Cao, T.D. Zhang, T.R.G.L. Bai, Y. Yu, Y.F. Hou, Y. Feng, W.D. Fei, Ceram. Int. **42**, 14788–14792 (2016)
21. J. Yan, G.D. Hu, X.M. Chen, W.B. Wu, C.H. Yang, J. Appl. Phys. **104**, 076103 (2008)
22. M.D. Chermahini, I. Safaee, M. Kazazi, M.M. Shahraki, Ceram. Int. **44**, 14281–14285 (2018)
23. G.D. Hu, S.H. Fan, C.H. Yang, W.B. Wu, Appl. Phys. Lett. **92**, 192905 (2008)
24. Y.Q. Guo, P. Xiao, R. Wen, Y. Wan, Q.J. Zheng, D.L. Shi, K.H. Lam, M.L. L, D.M. Lin, J. Mater. Chem. C **3**, 5811–5824 (2015)
25. X.B. Xie, S.J. Yang, F.Q. Zhang, S.H. Fan, Q.D. Che, C.J. Wang, X.D. Guo, L.P. Zhang, J. Mater. Sci.: Mater. Electron. **26**, 10095–10101 (2015)
26. P. Du, F. Yang, X.M. Zang, C.C. Qiu, J. Mater. Sci.: Mater. Electron. **25**, 5316–5321 (2014)
27. J.D. Yan, M. Gomi, T. Hattori, T. Yokota, H.H. Song, Thin Solid Films **542**, 150–154 (2013)
28. Y.B. Zi, X.L. Jiao, H.F. Wang, Q.Z. Liu, Z.Z. Yin, F.H. Zhang, Z. Huang, W.B. Wu, Chin. J. Phys. **31**, 280–285 (2009)
29. D. Li, W.C. Zheng, D.X. Zheng, J.L. Gong, L.Y. Wang, C. Jin, P. Li, H.L. Bai, ACS Appl. Mater. Interfaces **8**, 3977–3984 (2016)
30. A.R. Makhdoom, M.J. Akhtar, M.A. Rafiq, M. Siddique, M. Iqbal, M.M. Hasan, AIP Adv. **4**, 037113 (2014)
31. C.M. Raghavan, D. Do, J.W. Kim, W.J. Kim, S.S. Kim, J. Am. Ceram. Soc. **95**, 1933–1938 (2012)
32. J.G. Wu, J. Wang, D.Q. Xiao, J.G. Zhu, J. Am. Ceram. Soc. **94**, 4291–4298 (2011)
33. C.M. Raghavan, J.W. Kim, S.S. Kim, J. Am. Ceram. Soc. **97**, 235–240 (2014)
34. C.M. Raghavan, J.W. Kim, S.S. Kim, Ceram. Int. **40**, 2281–2286 (2014)
35. P. Padmini, T.R. Taylor, M.J. Lefevre, A.S. Nagra, R.A. York, J.S. Speck, Appl. Phys. Lett. **75**, 3186 (1999)